



ELSEVIER

Available online at www.sciencedirect.com

SCIENCE @ DIRECT®

Optics Communications 216 (2003) 25–31

OPTICS
COMMUNICATIONS

www.elsevier.com/locate/optcom

Off-axis aberration compensation of focusing with spherical mirrors using deformable mirrors

Thomas A. Planchon*, Pascal Mercère, Gilles Chériaux, Jean-Paul Chambaret

Laboratoire d'Optique Appliquée, Ecole Nationale Supérieure des Techniques Avancées, Ecole Polytechnique, CNRS UMR 7639 Chemin de la Hunière, 91761 Palaiseau cedex, France

Received 30 August 2002; received in revised form 12 November 2002; accepted 6 December 2002

Abstract

We studied the possibility of focusing an ultra-intense laser beam with a spherical mirror instead of a parabolic mirror. To correct the induced wavefront aberrations, we used a deformable mirror in a closed-loop configuration with a Shack–Hartmann Wavefront Sensor (SHWS). We demonstrate in this paper that we were able to correct the aberrations induced by spherical mirrors down to an f -number equal to 3.3.

© 2002 Elsevier Science B.V. All rights reserved.

1. Introduction

In ultra-intense laser chains, the propagation of the laser beam through many optical components, and thermal effects during the amplification processes, produces spatial aberrations onto the beam. These aberrations affect the focal spot of the beam, and should be reduced or corrected in order to minimize the size of this focal spot and thus increase the peak intensity of the laser when it is focused [1].

In the case of Ti:sapphire laser chains, spatial aberrations due to thermal effects in power amplifiers can be corrected by cooling the Ti:sapphire crystal down to 120 K [2]. At this temperature, its

thermal conductivity is largely increased. Spatial filtering between each amplifier stage also helps in keeping a good beam quality. However, spatial filtering does not suppress low-order aberrations such as astigmatism, and it is difficult to implement at high energy levels (above 50–100 mJ in picosecond regime). Finally, at the end of ultra-intense lasers, the residual wavefront aberrations can also be corrected by use of an adaptive optics system.

After compression, the beam is generally focused on target by an off-axis parabolic mirror. Our idea was to replace this standard high numerical aperture off-axis parabolic mirror by a spherical mirror, and then correct the induced aberrations by a deformable mirror, already implemented in this kind of lasers. Indeed deformable mirrors are increasingly used in ultra-intense laser chains for correction of wavefront aberrations [3–5], thus it appears natural to use adaptive

* Corresponding author. Tel.: +33-1-69-31-99-01; fax: +33-1-69-31-99-96.

E-mail address: thomas.planchon@enstey.ensta.fr (T.A. Planchon).

optics in order to correct the aberrations of an off-axis focusing spherical mirror.

Focusing this type of laser with a spherical mirror would lead to some advantages. Spherical mirrors can have smaller focal lengths than parabolic mirrors, can be manufactured accurately, and can allow for larger flexibility to the laser at about equal cost (several f -numbers can be realized because of the inexpensive spherical mirror).

Three spherical mirrors were investigated, with f -numbers from 6.7 down to 3.3. The laser is running in a closed-loop configuration using a bimorph deformable mirror and a 32 by 32 sub-pupil Shack–Hartmann Wavefront Sensor (SHWS). The commercially available software (Imagine Optic) calculates voltages to be applied onto the deformable mirror in order to correct the wavefront measured by the SHWS.

2. Experimental set-up

A schematic diagram of the experimental set-up is shown in Fig. 1. The experiment was performed with an attenuated beam of the 10 Hz/100 TW CPA laser chain.

The beam is sent onto the deformable mirror and is then focused by a spherical mirror working in an off-axis configuration. The deformable mirror is relay-imaged onto the SHWS pupil by using two doublet lenses. Doublets were taken in order to minimize aberrations given by the imaging system on the SHWS measurement. A cube beamsplitter enabled us to simultaneously perform wavefront measurements with the SHWS and far field analysis on a CCD camera, which exhibits a linear response ($\gamma = 1$). The observation of this far field pattern on the CCD camera is implemented to observe the effect of the wavefront correction.

The comparison between a plate beamsplitter and a cube beamsplitter was also studied. While the plate beamsplitter introduces coma aberration on the transmitted beam and not on the reflected one, we note a perfect similarity between the two beams splitted by the cube beamsplitter. For that reason, the experiments were performed with the cube beamsplitter.

The incident beam was 60 mm in diameter. We tested three different spherical mirrors ($R = 800$, 600, and 400 mm), corresponding to f -numbers 6.7, 5, and 3.3, respectively (f -number = f/D is

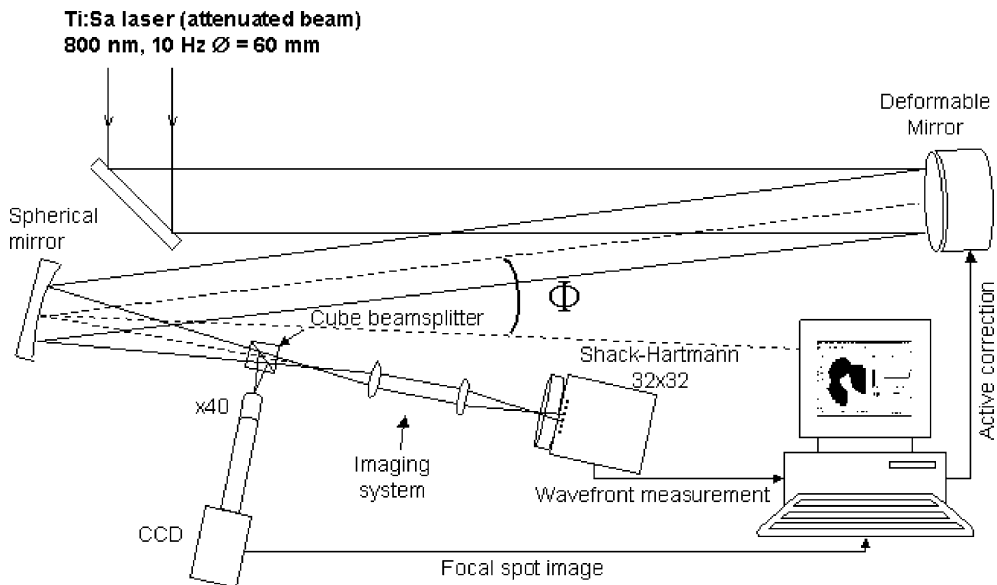


Fig. 1. Experimental set-up.

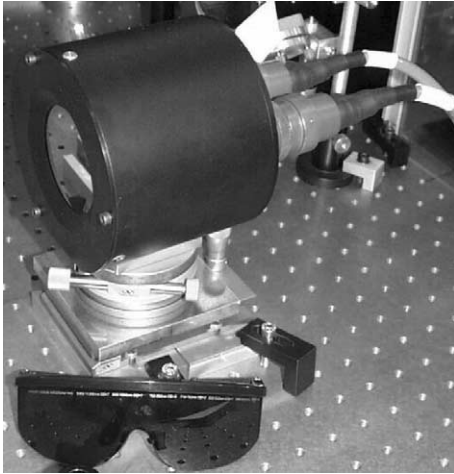


Fig. 2. The CILAS BIM 36 bimorph mirror.

also noted $f/\#$). The field angles on spherical mirrors were $\Phi = 4^\circ$, 4° , and 6° , respectively.

We are using a deformable mirror manufactured by CILAS Company [6] called BIM36 (see Figs. 2 and 9). This bimorph mirror has 36 actuators (made of piezoelectric material) and exhibits an excursion range of $\pm 40 \mu\text{m}$ when working on focus mode.

This silver coated BIM36 is usable over an aperture diameter of 60–64 mm. The applied voltages can reach $\pm 400 \text{ V}$. A major advantage of this device is that the radius of curvature induced in the mirror surface, in the region of an actuator, is linear with the applied voltage on this actuator.

3. Structure of the adaptive optics algorithm

The procedure needed to achieve a correction is as follows. For a more precise description of this process, the reader is invited to see [7].

First, the uncorrected wavefront is recorded. This wavefront, after removing tilt and focus terms, also includes the defects of the deformable mirror itself.

Then we determine the response function of the deformable mirror. For each actuator, voltages of $\pm 100 \text{ V}$ are applied and the resulting wavefronts are measured. At this point, it is important to relay-image the surface of the de-

formable mirror onto the SHWS. By doing so, we get the same wavefront (with a magnification factor) on the mirror and on the SHWS, and above all we keep the pupil constant on the wavefront sensor for each applied voltage. These measurements are used to construct an interaction matrix.

Matrix calculations then permit us to obtain, with the interaction matrix, the command matrix for the correction. This command matrix gives the right voltage to be applied to each actuator to induce a specific deformation onto the wavefront.

In the operating regime, the loop software calculates (by use of the former command matrix) the voltages to be applied for wavefront correction, which is achieved in one single iteration. The inverse wavefront of the initial aberrated wavefront measured by SHWS is directly reconstructed onto the bimorph mirror.

4. Results and discussion

4.1. Calculation of the Strehl ratio

In order to characterize the spatial quality of the beam, we use the Strehl ratio (SR) criterion defined as follows:

$$\text{SR} = \frac{\text{peak intensity at focus of the real beam}}{\text{peak intensity at focus of a reference beam}}$$

The classical definition considers a flat intensity and phase over the whole pupil for the reference beam, but it is more suitable for CPA laser system to use either a gaussian or the experimental intensity profile itself [1] with a flat wavefront for the reference.

All Strehl ratio values given in this paper are calculated from SHWS measurements. Peak intensity values are obtained by calculating the point spread function (PSF) of the beam, which is the bidimensional Fourier transform of the spatial intensity profile taking into account the wavefront. It means that with this Strehl ratio definition, we only get a criterion that qualifies the wavefront quality of the beam. So if no aberration is present on the wavefront, the Strehl ratio value is 1.

4.2. Measurement of the aberrated wavefront

The initial laser aberrations are rather small compared to the ones produced by the spherical mirrors themselves. Measurements of the aberrated wavefronts are shown in Fig. 3 for all spherical mirrors. These wavefronts are shown after numerical suppression of tilt and focus terms. The wavefront distortions are given in terms of peak-to-valley (PV) and root-mean-square (RMS).

For a measurement, if we note $\varphi(i)$ the phase value for the sub-pupil “ i ” and N the number of illuminated sub-pupils of the SHWS, then the RMS value σ is given by

$$\sigma = \text{RMS} = \sqrt{\frac{1}{N} \sum_{i=1}^N [\varphi(i) - \langle \varphi(i) \rangle]^2}$$

The RMS value of φ measures the dispersion of φ around its mean value, which is zero in our case. It is to be noted that for small aberrations we can express the Strehl ratio as follows [8], with

the RMS value σ and the wavelength λ given in meters:

$$\text{SR} = 1 - \left(\frac{2\pi}{\lambda}\right)^2 \times \sigma^2$$

The measured wavefronts can be expanded in term of Zernike polynomials for circular pupils [9], giving a direct access to the aberration coefficients. With this analysis, we see that the dominant aberrations for the three wavefronts are astigmatism and coma in the incident plane. The primary aberration coefficients are shown in Fig. 4.

4.3. Wavefront correction

Corrected wavefronts are presented in Fig. 5. The z scale on these measured wavefronts is enlarged (in comparison with the z scale of wavefronts before correction shown in Fig. 3) by a factor of ten in order to see the residual aberrations (main aberration coefficients are shown in Fig. 4). As we can see, astigmatism and coma

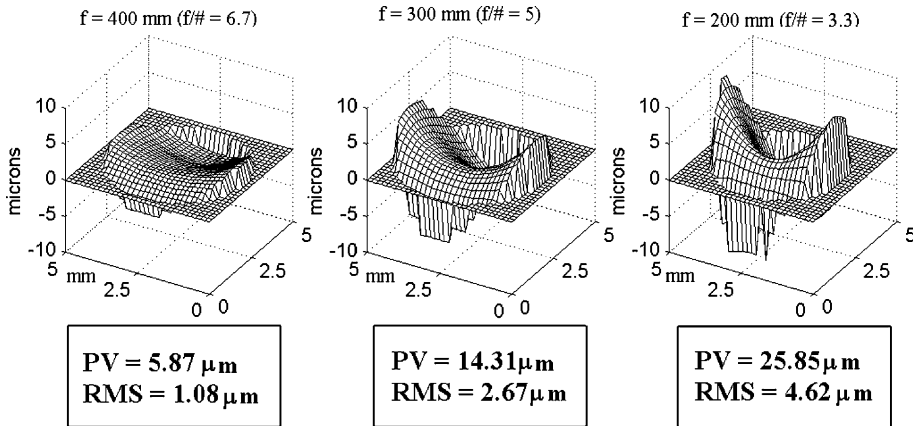


Fig. 3. 3D representations of the aberrated wavefronts for the three spherical mirrors.

Spherical mirror	(f/#) = 6.66		(f/#) = 5		(f/#) = 3.33	
	Before correction	After correction	Before correction	After correction	Before correction	After correction
astigmatism at 0°	2.501	0.048	6.114	0.023	10.343	0.048
astigmatism at 45°	0.005	-0.003	0.116	0.003	-0.633	-0.003
coma at 0°	0.020	-0.026	-0.013	-0.024	-0.292	-0.026
coma at 90°	-0.914	0.075	-2.121	0.042	-4.965	0.075
3rd order spherical aberration	-0.028	0.029	-0.125	0.035	-0.541	0.029

Fig. 4. Primary Zernike aberration coefficients for the three spherical mirrors given in microns.

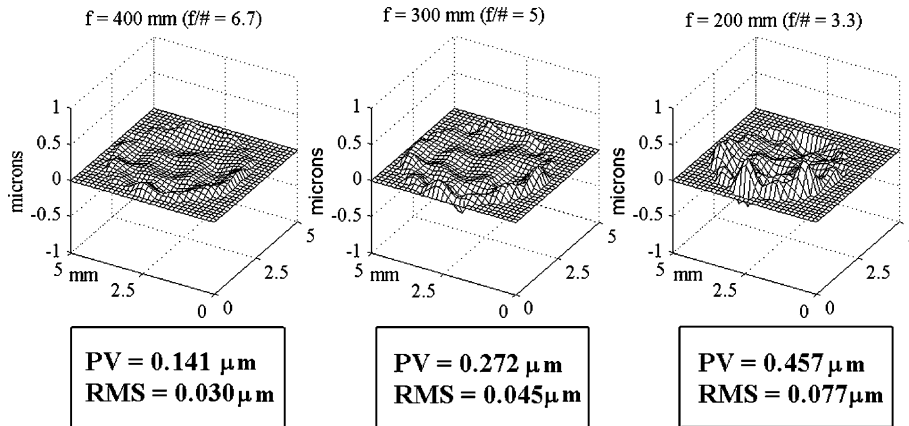


Fig. 5. 3D representations of the corrected wavefronts for the three spherical mirrors.

produced by the spherical mirror are well corrected. Only a small amount of higher order aberrations remains, corresponding to residuals phase aberrations induced by the deformable mirror, and higher order aberrations that the deformable mirror is not able to correct.

After correction, the PV and RMS values are reduced by a factor of 40–60. We notice that we

are close to the mirror flatness limit, which was measured to be 20 nm RMS.

This experiment shows that the replacement of a parabolic mirror by a spherical one is acceptable for an f -number as small as 3.3. For the third spherical mirror ($f/\# = 3.3$, $f = 200$ mm), the angle Φ was made as small as possible ($\Phi = 6^\circ$). We were near the maximally acceptable voltage of ± 400 V on two actuators (see Fig. 6). So it appears that if we want to correct the distortions induced when focusing with a spherical mirror of shorter focal length, the deformable mirror would need a wider excursion range. Finally, the table below shows the Strehl ratios obtained for each spherical mirror tested (Fig. 7).

4.4. Focal spot imaging and point spread function

The corrections we achieved are very satisfying. We directly observed the effect of the wavefront correction onto the focal spot image given by the CCD camera. The calculated PSF are in very good agreement with the measured focal spots (see Fig. 8).

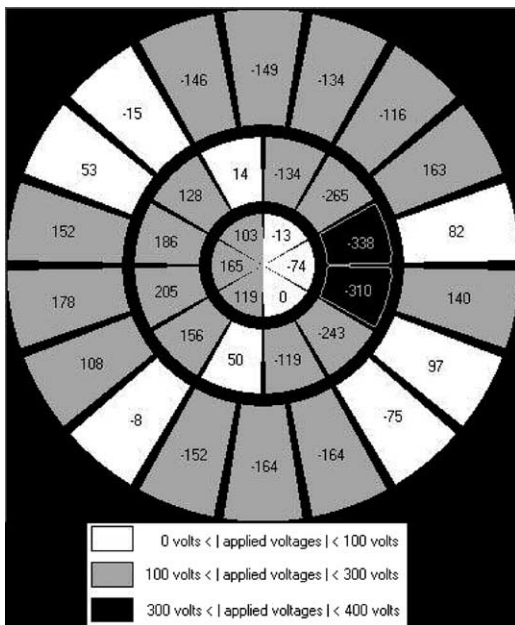


Fig. 6. Applied voltage for correction with spherical mirror with $f/\# = 3.3$.

Spherical mirror	$f/\# = 6.7$	$f/\# = 5$	$f/\# = 3.3$
Before correction	0.10	0.02	0.01
After correction	0.94	0.89	0.71

Fig. 7. Strehl ratio values.

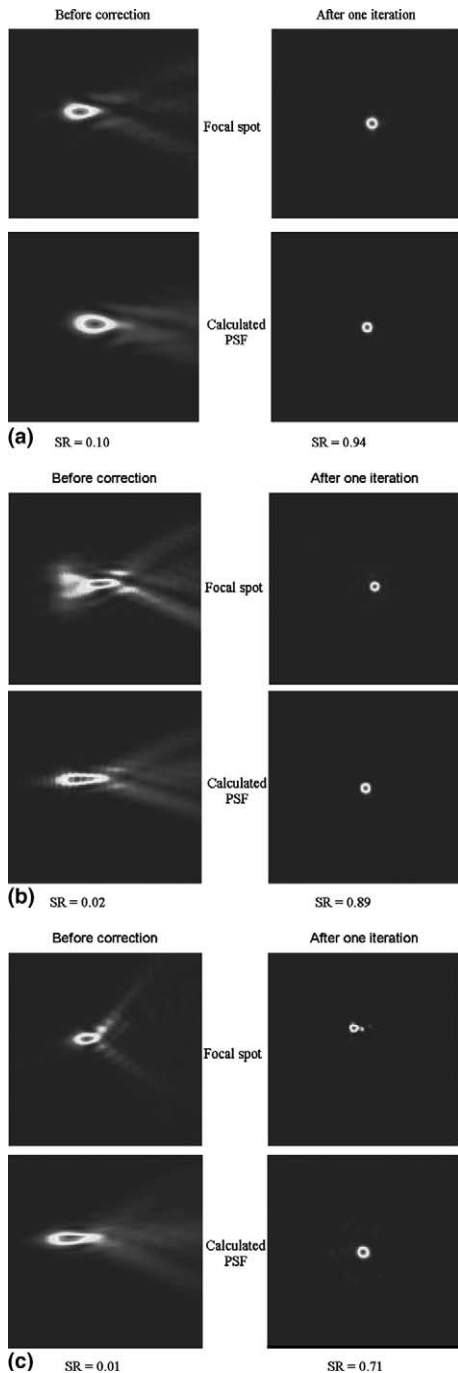


Fig. 8. Focal spot – before and after correction – seen by the CCD camera and calculated by the SHWS: spherical mirror (a) $f/\# = 6.66$; (b) $f/\# = 5$; (c) $f/\# = 3.33$.

5. Influence of spherical aberration

While conducting the experiment, we noticed that the spherical aberration was a key factor obtaining a good correction.

We observed that if the bimorph mirror has to correct only astigmatism or coma, the residual phase aberrations after correction are small, but when the bimorph mirror has to correct also spherical aberration, then the residual aberrations are much greater.

These residual distortions are due to the voltage distribution on the actuators. When correcting spherical aberration, the central actuators and the first ring of actuators exhibit voltages with opposite sign, because of the shape of spherical aberration. For each central actuator, we can see on Fig. 9 that the voltage is also applied in the space between two adjacent actuators of the first ring. This opposite voltage leads to mechanical defects onto the mirror surface.

In order to check this limitation, we made another experiment with a slightly different experimental set-up, which allowed us to induce spherical

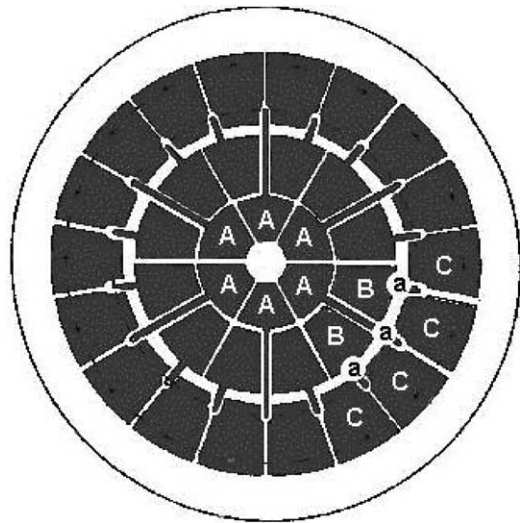


Fig. 9. Distribution of actuators on BIM36 mirror: (A) 6 central actuators; (B) 12 actuators on first ring; (C) 18 actuators on second ring; (a) area where voltages are applied for actuators A and B.

aberration by replacing a $f = 500$ mm doublet by a $f = 500$ mm plano-convex singlet lens.

With the doublet lens, the remaining value was 32 nm RMS for the corrected wavefront, which gave a Strehl ratio of 0.93. With the singlet lens (others aberration coefficients, mainly astigmatism, were nearly the same), we end up with 161 nm RMS, which gave a Strehl ratio of 0.08. At the same time, on the focal spot image, we clearly saw a hexagonal structure in relation to the electrode pattern.

6. Conclusions

In order to demonstrate the possibility of correcting the aberrated wavefront of a beam focused by a spherical mirror used in an off-axis configuration, we successfully used a closed loop with a Shack–Hartmann wavefront sensor combined with a bimorph deformable mirror.

A CCD camera was used to compare the real focal spot with the one deduced from SHWS measurement. This comparison confirmed our results. The wavefront distortions are reduced by a factor of 40–60 by the adaptive optics loop. The Strehl ratios are very good after correction, and the PSF calculations are in good agreement with the focal spot images given by the CCD camera.

From this study, it appears that with our deformable mirror (bimorph 36 actuators from CI-

LAS), the minimum f -number for spherical mirror is 3.3. It was obtained for a focal length of $f = 200$ mm with an incident angle of 6° .

Acknowledgements

We would like to thank Europe for support, this work was part of an European RTD program ADAPTOOL (#HPRI-CT-1999-50012).

References

- [1] S. Ranc, G. Chériaux, S. Ferré, J.-P. Rousseau, J.-P. Chambaret, *App. Phys. B* 70 (2000) S181.
- [2] M. Pittman, S. Ferré, J.P. Rousseau, L. Notebaert, J.P. Chambaret, G. Chériaux, *App. Phys. B* 74 (6) (2002) 529.
- [3] K. Akaoka, S. Harayama, K. Tei, Y. Maruyama, T. Arisawa, *SPIE* 3265 (1998) 2219.
- [4] F. Druon, G. Chériaux, J. Faure, J. Nees, M. Nantel, A. Maksimchuk, G. Mourou, J.C. Chanteloup, G. Dovin, *Opt. Lett.* 23 (13) (1998) 1043.
- [5] M.D. Perry, D. Pennington, B.C. Stuart, G. Titbohl, J.A. Britten, C. Brown, S. Herman, B. Golick, M. Kartz, J. Miller, H.T. Powell, M. Vergino, V. Yanovsky, *Opt. Lett.* 24 (3) (1999) 160.
- [6] P. Jagourel, C. Maennel, J.-C. De Miscault, *Proc. SPIE*, Vol. 3885 in: High Power ablation II (2000) 530.
- [7] J.W. Hardy, *Adaptive Optics for Astronomical Telescopes*, Oxford University, Oxford, 1998, chapter 8.
- [8] J. Herrmann, *JOSA B* 9 (12) (1992) 2257.
- [9] J.Y. Wang, D.E. Silva, *Appl. Opt.* 19 (9) (1980) 1510.